Optics Letters

Room-temperature magnetic gradiometry with fiber-coupled nitrogen-vacancy centers in diamond

S. M. Blakley,[1] I. V. Fedotov,[1,2,3] S. Ya. Kilin,[3,4] and A. M. Zheltikov[1,2,3,*]

[1]Department of Physics and Astronomy, Texas A&M University, College Station, Texas 77843, USA
[2]Physics Department, International Laser Center, M. V. Lomonosov Moscow State University, Vorob'evy gory, Moscow 119992, Russia
[3]Russian Quantum Center, Moscow Region, Skolkovo 143025, Russia
[4]B. I. Stepanov Institute of Physics, National Academy of Sciences of Belarus, Minsk, Belarus
*Corresponding author: zheltikov@physics.tamu.edu

Received 7 April 2015; accepted 12 May 2015; posted 1 July 2015 (Doc. ID 237633); published 5 August 2015

Differential optical detection of a magnetic resonance induced in nitrogen–vacancy (NV) centers in diamond is shown to enable a high-spatial-resolution room-temperature magnetic-field gradiometry on a fiber platform. An ultracompact design of this fiber-based solid-state magnetic gradiometer is achieved by integrating an NV-diamond magnetic sensor with a two-fiber opto–microwave interface, which couples NV centers to microwave and optical fields, used to resonantly drive and interrogate the spin of NV centers.

OCIS codes: (060.2370) Fiber optics sensors; (230.3810) Magneto-optic systems; (060.2300) Fiber measurements.

http://dx.doi.org/10.1364/OL.40.003727

Nitrogen–vacancy (NV) centers in diamond [1–5] offer unique opportunities for high-sensitivity magnetic-field measurements at room temperature with unprecedented spatial resolution [6–8] and potentially attainable sensitivities comparable to those of SQUID magnetometers [9]. While the highest sensitivities of NV-diamond-based magnetic-field sensing and gradiometry have been achieved using confocal microscopy [10,11], optical fibers have been recently shown [11–13] to offer a missing link for a practical implementation of NV-diamond-based sensing in a variety of environments, including magnetic-field and temperature measurements in biological systems.

In real-life applications, weak magnetic fields from objects under study, e.g., a beating heart or firing neurons, need to be detected against a strong background due to the magnetic field of the Earth or technogenic environment. Atomic coherent effects in alkali-metal vapors have been shown to enable the creation of innovative ultrahigh-sensitivity magnetic gradiometers [14,15], allowing the magnetic field of the heart to be mapped with a high accuracy from outside the body [15,16]. However, because metal vapor preparation requires a specifically designed gas cell, the miniaturization of such magnetometers is limited, motivating a search for an all-solid-state design of a highly sensitive optical magnetometer.

Here, we demonstrate a versatile high-spatial-resolution solid-state magnetic gradiometer that operates on a fiber platform using the optically detected magnetic resonance in NV centers of diamond. An ultracompact design of this fiber-based magnetic gradiometer is achieved by integrating an NV-diamond magnetic sensor with a two-fiber opto-microwave interface, which couples NV centers to microwave and optical fields, used to resonantly drive and interrogate the spin of NV centers. This fiber-based magnetic gradiometer is shown to provide a spatial resolution below 0.5 mm and a magnetic-field sensitivity at the level of 60 $\mathrm{pT/Hz^{1/2}}$.

The fiber-optic magnetic gradiometer developed in this work consists of a bulk NV-center-enriched diamond particle, a pair of optical fibers attached to this diamond particle at two different locations, and a two-wire transmission line for the delivery of the microwave field. Two identical optical fibers, each having a core diameter of 200 μm, are attached, using a mechanical manipulator, to an NV-diamond particle with a diameter of about 1 mm (Fig. 1). The fibers are fixed to the NV-diamond sensor with a core-to-core separation $d \approx 480$ μm using ethyl cyanoacrylate glue [Fig. 2(a)].

The ground state of NV centers is a spin triplet, with $m_s = 0$ and $m_s = \pm 1$ states in the absence of an external magnetic field split by $\Omega_s \approx 2.87$ GHz. The laser pump, delivered by the optical fibers, spin-polarizes NV centers, accumulating them in the $m_s = 0$ state through spin-selective decay paths [6–8]. For NV centers in the $m_s = \pm 1$ state, the yield of photoluminescence (PL) within the 630–800-nm wavelength range induced by the same laser radiation is lower than that typical of NV centers in the $m_s = 0$ state, because a substantial fraction of the $m_s = \pm 1$ excited-state population is transferred to the $m_s = 0$ ground level via a metastable singlet state [the ^1A state in Fig. 2(a)]. Thus, when a microwave field

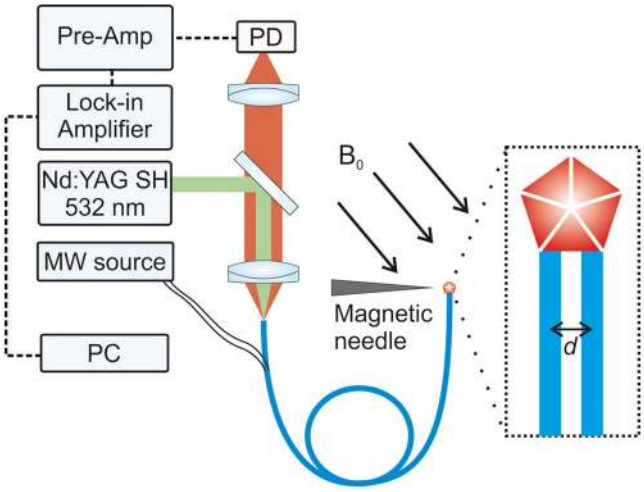

Fig. 1. Experimental setup: Nd:YAG SH, continuous-wave Nd:YAG laser with second-harmonic output; MW source, microwave source; PC, personal computer; PD, photodetector.

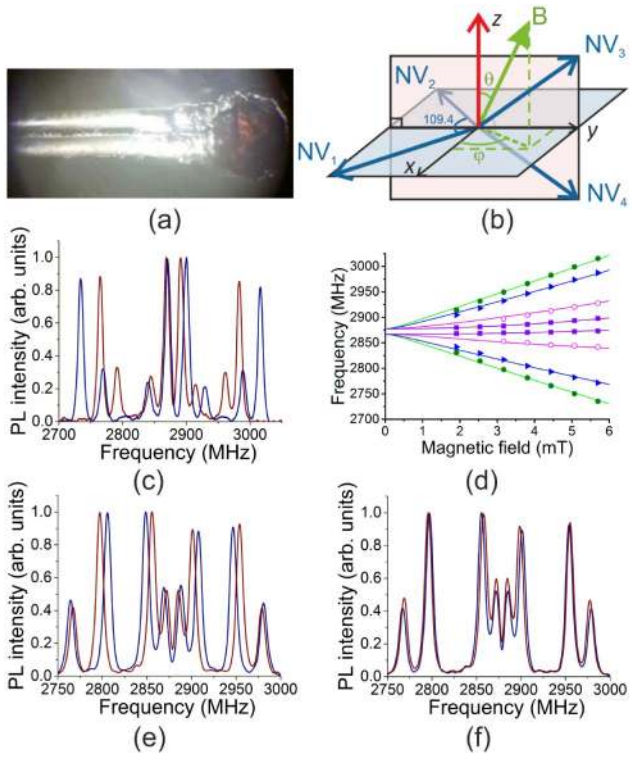

Fig. 2. (a) A fiber-based magnetic gradiometer integrating an NV-diamond sensor with a two-fiber opto–microwave interface. (b) An external magnetic field **B** versus the *x*-, *y*-, and *z*-coordinate axes related to the crystal lattice of diamond, with NV axes 1 and 2 lying in the *xy*-plane, the *z*-axis perpendicular to this plane, and the *y*-axis chosen along the bisector of the angle between NV axes 3 and 4 and belonging to the plane defined by these axes. (c) Typical ODMR spectra recorded through one of the two fiber channels of the fiber gradiometer in the presence of a homogeneous magnetic field $B_0 \approx 4.4$ mT (red line) and 5.7 mT (blue line). (d) The frequencies $\Omega_j (i = 1, 2, 3, 4)$ of the four pairs of the Zeeman-shifted peaks in the ODMR spectra plotted as a function of the magnitude of the magnetic field: (data points) experimental results and (solid lines) calculations. (e) ODMR spectra recorded through the same fiber channel of the fiber gradiometer probe with the spatially inhomogeneous component of the magnetic field switched on (red line) and off (blue line) with $B_0 \approx 4.1$ mT. (f) ODMR spectra recorded through the first (blue line) and second (red line) fiber channels of the fiber gradiometer in the presence of an external magnetic field $\mathbf{B} = \mathbf{B}_0 + \mathbf{B}_i$.

delivered by the two-wire transmission line is tuned to the zero-field splitting frequency Ω_s, transferring population from the $m_s = 0$ state to the $m_s = \pm 1$ sublevels, the intensity of the PL signal, I_{PL}, decreases. This effect is observed as a well-resolved feature in the PL intensity I measured as a function of the microwave frequency Ω. Even in the absence of external magnetic fields, a local strain removes the degeneracy of this resonance [6–8], giving rise to two well-resolved features in $I(\Omega)$ spectra.

To understand the properties of the ODMR $I(\Omega)$ spectra observed in experiments with an ensemble of NV centers ordered in the crystal lattice of diamond, we resort to the spin Hamiltonian of an NV center [7–9], $H_s = \mu_B\, g\, \mathbf{BS} + hD[S_Z^2 - S(S+1)/3] + hE(S_{X2} - S_{Y2})$, where μ_B is the Bohr magneton, h is the Planck constant, $g \approx 2$ is the electron g-ratio, **B** is the external magnetic field, D and E are the zero-magnetic-field splitting parameters, and $S_j (j = X, Y, Z)$ are the projections of the electron spin **S** on the principal Cartesian coordinate axes X, Y, Z, with the Z-axis chosen along the N–V axis. As shown in the earlier work [7–9,11], in the presence of a well-calibrated bias magnetic field, the external magnetic field **B** can be retrieved from four pairs of spectral features in the ODMR $I(\Omega)$ spectra observed at magnetic resonance frequencies corresponding to the projections of the field **B** on the four possible directions of N–V axes in the crystal lattice of diamond [Fig. 2(b)].

In experiments, an acousto-optical modulator is used to couple 50 mW of the 532-nm second-harmonic output of a cw Nd:YAG laser into each of the optical fibers attached to the NV-diamond sensor, thus providing a parallel optical excitation of NV centers at two different locations in diamond. The PL signal from NV centers is then collected by the same fibers, enabling differential ODMR measurements (Fig. 1). Each optical fiber is used to measure the PL signal from NV centers in diamond as a function of the frequency of the microwave field delivered through the two-wire transmission line, thus enabling a fiber-based differential optical detection of the magnetic resonance (ODMR) of NV centers. The gradient of an external magnetic field is then retrieved through a comparative analysis of ODMR spectra $I_1(\Omega)$ and $I_2(\Omega)$ recorded through the first and second optical fibers.

For high-speed, high-sensitivity differential ODMR measurements, a rectangular modulation with a frequency $f_m \approx 1.13$ kHz is applied to the frequency of the microwave voltage-controlled oscillator output using a digit-to-analog converter, controlled by homemade dedicated software. The frequency of the modulated microwave output changes periodically in a rectangular fashion from its minimum at 2.3 GHz to its maximum value scanned from 2.5 to 3.1 GHz. A lock-in amplifier is then used to retrieve a signal at $f_m \approx 1.13$ kHz from the overall PL return signal detected by a photodiode

and boosted by a preamplifier, thus discriminating the modulated spin readout against the constant PL background. A 14-bit analog-to-digital converter was used to digitize the results of measurements and analyze the recorded $I(\Omega)$ spectra.

In Fig. 2(c), we present typical ODMR spectra recorded through one of the two fiber channels of the fiber gradiometer in the presence of a homogeneous magnetic field $\mathbf{B}_0$ induced by a homebuilt solenoid, made of a 25.4-mm-diameter iron cylinder wrapped with 187 turns of 20-gauge copper magnet wire. The magnetic field induced by this solenoid is controlled by varying the dc current through the copper wire up to a maximum of 3 A. The ODMR spectra exhibit four well-resolved peaks at the frequencies of magnetic resonance, $\Omega_j (i = 1, 2, 3, 4)$, corresponding to four possible orientations of NV centers relative to the lattice of diamond [Fig. 2(b)]. As the external magnetic field is increased by increasing the electric current through the solenoid, all these magnetic resonances are shifted toward higher frequencies. As can be seen from Fig. 2(d), the frequencies Ω_i of the peaks in the ODMR spectra measured as functions of the external magnetic field B [data points in Fig. 2(d)] agree very well with the magnetic-resonance frequencies Ω_i calculated by solving the characteristic equation for the Hamiltonian H_s [solid lines in Fig. 2(d)], providing an accurate calibration curve for magnetic field measurements.

In the magnetic gradiometry mode, the fiber probe is employed to perform differential ODMR measurements in the presence of an external magnetic field consisting of a strong spatially homogeneous magnetic field $\mathbf{B}_0$ from the above-described solenoid and a weak spatially inhomogeneous magnetic field $\mathbf{B}_i$ induced by a magnetized 1-mm-diameter metal needle. In Fig. 2(e), we plot ODMR spectra recorded through the same fiber of our fiber probe with the spatially inhomogeneous component of the magnetic field switched on and off. The field $\mathbf{B}_i$ is seen to give rise to detectable changes in the ODMR spectra.

In Fig. 2(f) we present ODMR spectra $I_1(\Omega)$ and $I_2(\Omega)$ recorded through two fiber channels of the fiber gradiometer in the presence of an external magnetic field $\mathbf{B} = \mathbf{B}_0 + \mathbf{B}_i$. In this experiment, the fiber magnetometer is placed at a distance of about 1 cm from the tip of the magnetized needle and oriented in such a way that only the magnitude of the magnetic field, but not its direction, changes from one fiber channel to another. The magnitudes of the magnetic field retrieved from the $I_1(\Omega)$ and $I_2(\Omega)$ ODMR spectra presented in Fig. 2(f) are $B_1 \approx 0.35$ mT and $B_2 \approx 0.41$ mT, corresponding to a magnetic field gradient $|\Delta B/d| \approx 0.12$ mT/mm.

Figures 3(a)–3(d) display the results of experiments, where the fiber gradiometer was placed at a distance of 1–2 mm from the tip of the magnetized needle. In such an experimental arrangement, not only the magnitude, but also the direction of the magnetic field changes from one fiber channel of the fiber gradiometer to another. Measurements performed with and without the spatially homogeneous component of the magnetic field are shown by red and blue lines, respectively. The spatially inhomogeneous component of the magnetic field retrieved from the ODMR spectra is $B_i \approx 1.4$ mT, $\theta_i \approx 3.2°$, $\phi_i \approx 50°$ [Figs. 3(a) and 3(c)] and $B_i \approx 1.1$ mT, $\theta_i \approx 80°$, $\phi_i \approx 2.0°$ [Figs. 3(b) and 3(d)] for measurements performed through the first fiber channel and $B_i \approx 1.2$ mT, $\theta_i \approx 7.4°$, $\phi_i \approx 67°$ [Figs. 3(a) and 3(c)] and $B_i \approx 1.3$ mT, $\theta_i \approx 60°$, $\phi_i \approx 7.4°$ [Figs. 3(b) and 3(d)] when measured through the second fiber channel. The magnetic fields retrieved from the ODMR spectra and the respective field gradients agree very well with the results of calculations for the magnetic field $\mathbf{B}$ induced in this experimental geometry.

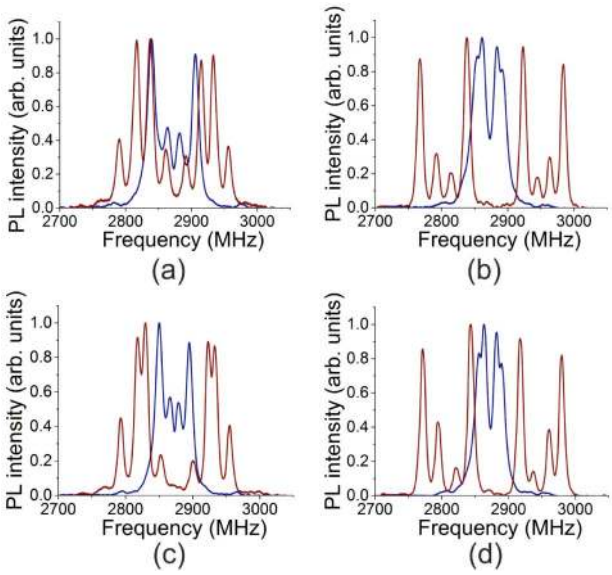

Fig. 3. ODMR spectra recorded through the first (a), (b) and second (c), (d) fiber channels of the fiber gradiometer in the presence of an external magnetic field $\mathbf{B} = \mathbf{B}_0 + \mathbf{B}_i$ consisting of a spatially homogeneous component with $B_0 = 0$ (blue lines) and $B_0 \approx 4.4$ mT, $\theta_0 \approx 78°$, $\phi_0 \approx 11°$ (red lines) and a spatially inhomogeneous component with $B_i \approx 1.4$ mT, $\theta_i \approx 3.2°$, $\phi_i \approx 50°$ (a), (c) and $B_i \approx 1.1$ mT, $\theta_i \approx 80°$, $\phi_i \approx 2.0°$ (b), (d) at the location of the first fiber channel.

The limiting sensitivity of magnetic-field detection provided by the fiber gradiometer demonstrated in our experiments is estimated as [17] $\delta\eta \approx \sigma\hbar\Delta\nu(Cg\mu_B)^{-1}R^{-1/2}$, where σ is the line shape factor, $\Delta\nu$ is the full width at half-maximum of the ODMR line, C is the ODMR contrast, and R is the PL photon count rate. For the parameters of our system, $\sigma \approx 0.7$, $C \approx 0.05$, and $\Delta\nu \approx 8$ MHz, we find, assuming a laser power of 100 mW, the density of NV centers of $3 \cdot 10^{18}$ cm^{-3}, and the numerical aperture of the fiber channels $N \approx 0.4$, that $\delta\eta \approx 60$ pT/Hz$^{1/2}$. At this level of sensitivity, the fundamental features of magnetocardiogram of a human heart, whose typical amplitude is about 100 pT, can be detected with an integration time τ of less than 1 s. For the above-specified set of parameters, the lowest magnetic field gradient that can be detected using the fiber magnetic gradiometer demonstrated in this work, that is, with a spatial resolution of $d \approx 0.5$ mm and with $\tau \approx 1$ s $\delta B/d \approx 120$ pT/mm. Even lower magnetic field gradients can be detected at a cost of spatial resolution. Specifically, in magnetocardiography of human heart, where a resolution of 5–6 mm would be adequate, magnetic field gradients as low as 10–12 pT/mm could be detected, offering an attractive alternative to magnetic gradiometers based on alkali metal vapor cells.

To summarize, we have demonstrated a versatile high-spatial-resolution solid-state magnetic gradiometer that operates on a fiber platform using the optically detected magnetic resonance in NV centers of diamond. An ultracompact design of this fiber-based magnetic gradiometer is achieved by integrating an NV-diamond magnetic sensor with a two-fiber opto–microwave interface, which couples NV centers to microwave and optical fields, used to resonantly drive and interrogate the spin of NV centers. This fiber-based magnetic gradiometer is shown to provide a spatial resolution below 0.5 mm and a magnetic-field sensitivity at the level of 60 $pT/Hz^{1/2}$.

Funding. Russian Foundation for Basic Research (13-02-01465, 13-04-40335, 14-02-90030, 14-22-02100, 14-29-07182); Russian Science Foundation (14-12-00772); Welch Foundation (A-1801).

Acknowledgment. We are grateful to N. A. Safronov for valuable help in the automation of the experiment.

REFERENCES

1. T. Gaebel, M. Domhan, I. Popa, C. Wittmann, P. Neumann, F. Jelezko, J. R. Rabeau, N. Stavrias, A. D. Greentree, and S. Prawer, Nat. Phys. **2**, 408 (2006).
2. L. Childress, M. V. G. Dutt, J. M. Taylor, A. S. Zibrov, F. Jelezko, J. Wrachtrup, P. R. Hemmer, and M. D. Lukin, Science **314**, 281 (2006).
3. M. G. Dutt, L. Childress, L. Jiang, E. Togan, J. Maze, F. Jelezko, A. S. Zibrov, P. R. Hemmer, and M. D. Lukin, Science **316**, 1312 (2007).
4. I. Aharonovich, A. D. Greentree, and S. Prawer, Nat. Photonics **5**, 397 (2011).
5. A. Gruber, A. Dräbenstedt, C. Tietz, L. Fleury, J. Wrachtrup, and C. von Borczyskowski, Science **276**, 2012 (1997).
6. J. R. Maze, P. L. Stanwix, J. S. Hodges, S. Hong, J. M. Taylor, P. Cappellaro, L. Jiang, M. G. Dutt, E. Togan, A. S. Zibrov, A. Yacoby, R. L. Walsworth, and M. D. Lukin, Nature **455**, 644 (2008).
7. G. Balasubramanian, I. Y. Chan, R. Kolesov, M. Al-Hmoud, J. Tisler, C. Shin, C. Kim, A. Wojcik, P. R. Hemmer, A. Krueger, T. Hanke, A. Leitenstorfer, R. Bratschitsch, F. Jelezko, and J. Wrachtrup, Nature **455**, 648 (2008).
8. D. Le Sage, K. Arai, D. R. Glenn, S. J. DeVience, L. M. Pham, L. Rahn-Lee, M. D. Lukin, A. Yacoby, A. Komeili, and R. L. Walsworth, Nature **496**, 486 (2013).
9. J. M. Taylor, P. Cappellaro, L. Childress, L. Jiang, D. Budker, P. R. Hemmer, A. Yacoby, R. Walsworth, and M. D. Lukin, Nat. Phys. **4**, 810 (2008).
10. G. Kucsko, P. C. Maurer, N. Y. Yao, M. Kubo, H. J. Noh, P. K. Lo, H. Park, and M. D. Lukin, Nature **500**, 54 (2013).
11. I. V. Fedotov, L. V. Doronina-Amitonova, A. A. Voronin, A. O. Levchenko, S. A. Zibrov, D. A. Sidorov-Biryukov, A. B. Fedotov, V. L. Velichansky, and A. M. Zheltikov, Sci. Rep. **4**, 5362 (2014).
12. I. V. Fedotov, L. V. Doronina-Amitonova, D. A. Sidorov-Biryukov, N. A. Safronov, S. Blakley, A. O. Levchenko, S. A. Zibrov, A. B. Fedotov, S. Y. Kilin, M. O. Scully, V. L. Velichansky, and A. M. Zheltikov, Opt. Lett. **39**, 6954 (2014).
13. I. V. Fedotov, S. Blakley, E. E. Serebryannikov, N. A. Safronov, V. L. Velichansky, M. O. Scully, and A. M. Zheltikov, Appl. Phys. Lett. **105**, 261109 (2014).
14. C. Affolderbach, M. Stähler, S. Knappe, and R. Wynands, Appl. Phys. B **75**, 605 (2002).
15. G. Bison, R. Wynands, and A. Weis, Opt. Express **11**, 904 (2003).
16. G. Bison, R. Wynands, and A. Weis, Appl. Phys. B **76**, 325 (2003).
17. A. Dréau, M. Lesik, L. Rondin, P. Spinicelli, O. Arcizet, J.-F. Roch, and V. Jacques, Phys. Rev. B **84**, 195204 (2011).